Journal of the Korean Physical Society, Vol. 68, No. 5, March 2016, pp. 686∼691

Electrical Properties of $Mg_xZn_{1-x}O$ Thin Films Deposited by using RF Magnetron Co-sputtering with ZnO and $Mg_{0.3}Zn_{0.7}O$ Targets

Li Li YUE, Yi Da YANG and Hong Seung KIM*
Department of Electronic Material Engineering, Korea Maritime and Ocean University, Busan 49112, Korea

Nak Won JANG
Division of Electrical and Electronics Engineering,
Korea Maritime and Ocean University, Busan 49112, Korea

Young YUN
Division of Radio Communication Engineering, Korea Maritime and Ocean University, Busan 49112, Korea

(Received 18 December 2015, in final form 19 January 2016)

We successfully deposited hexagonal wurtzite $Mg_xZn_{1-x}O$ ($0 \leq x \leq 0.18$) films on Si substrates by using RF magnetron co-sputtering with ZnO and $Mg_{0.3}Zn_{0.7}O$ targets. The Mg content was varied by controlling the RF power of the $Mg_{0.3}Zn_{0.7}O$ target while the RF power of the ZnO target was fixed at 100 W. The electrical properties of the $Mg_xZn_{1-x}O$ films were investigated by using a transmission line model (TLM) with Ti/Au electrode and Hall effect measurements. The X-ray diffraction (XRD) results demonstrate that some Zn atoms can be replaced by Mg atoms in the $Mg_xZn_{1-x}O$ films. As the Mg content was increased from 0 at.% to 18 at.%, the resistivity of $Mg_xZn_{1-x}O$ films increased and the carrier concentration decreased from 1.17×10^{19} cm^{-3} to 1.17 $\times$ 10^{17} cm^{-3}, which indicates a decrease in the number of oxygen vacancies. Meanwhile, the Hall mobility increased to 15.3 cm^2/Vs. The electrical properties of $Mg_xZn_{1-x}O$ films were tuned by using the Mg content.

PACS numbers: 73.61.Ga, 73.61.-r, 81.15.Cd
Keywords: $Mg_xZn_{1-x}O$, Thin film, Electrical property, RF magnetron co-sputtering
DOI: 10.3938/jkps.68.686

I. INTRODUCTION

Zinc oxide (ZnO), as a wide band-gap (3.37 eV) compound semiconductor with a large exciton binding energy (60 meV), has been investigated for its potential application in optoelectronic devices, gas and chemical sensors, and transistors [1–3]. Ternary $Mg_xZn_{1-x}O$, as one kind of ZnO alloy, has received much attention for its potential application in deep-ultraviolet optoelectronic devices [4]. The band gap of $Mg_xZn_{1-x}O$ can be tuned from 3.37 eV to 7.8 eV [5], which covers a broad portion of the deep-ultraviolet spectrum range. Moreover, compared with other wide band-gap semiconductors, $Mg_xZn_{1-x}O$ has various unique features, such as a high resistance to radiation, an environmentally-friendly character, an amenability to conventional wet chemistry etching, and relatively low growth temperatures. However, the large crystal structure dissimilarity between wurtzite-hexagonal ZnO and rock-salt-cubic MgO leads to unstable phase mixing [6]. In the phase diagram of the ZnO-MgO binary system, the thermodynamic solubility limit of MgO in ZnO is only 4 at.% [7]. $Mg_xZn_{1-x}O$ films grown via pulsed laser deposition (PLD) were found to exceed the low solubility limit of MgO in ZnO due to the thermodynamic growth conditions, and single-phase films with a wurtzite structure of up to 33 at.% Mg were achieved [8]. Other deposition techniques have also been proposed to prepare $Mg_xZn_{1-x}O$ film, such as chemical vapor deposition [9], the sol-gel method technique [10], and radio-frequency (RF) magnetron sputtering [11]. Among these methods, RF magnetron sputtering is preferred due to its low cost, simplicity, and low process temperature. Compared with the sputtering method with a single MgZnO target with a fixed Mg composition, co-sputtering has a superior advantage. That is, $Mg_xZn_{1-x}O$ films with various Mg contents can be deposited with only two targets, and the Mg content can be varied by controlling the power or the area of target. Kar *et al.* [12] grew $Mg_xZn_{1-x}O$ ($x =$ 0.03) nanowires on a ZnO buffer layer by co-sputtering with ZnO and Mg targets. Kim *et al.* [11] fabricated a

*E-mail: hongseung@kmou.ac.kr; Fax: +82-51-404-3986

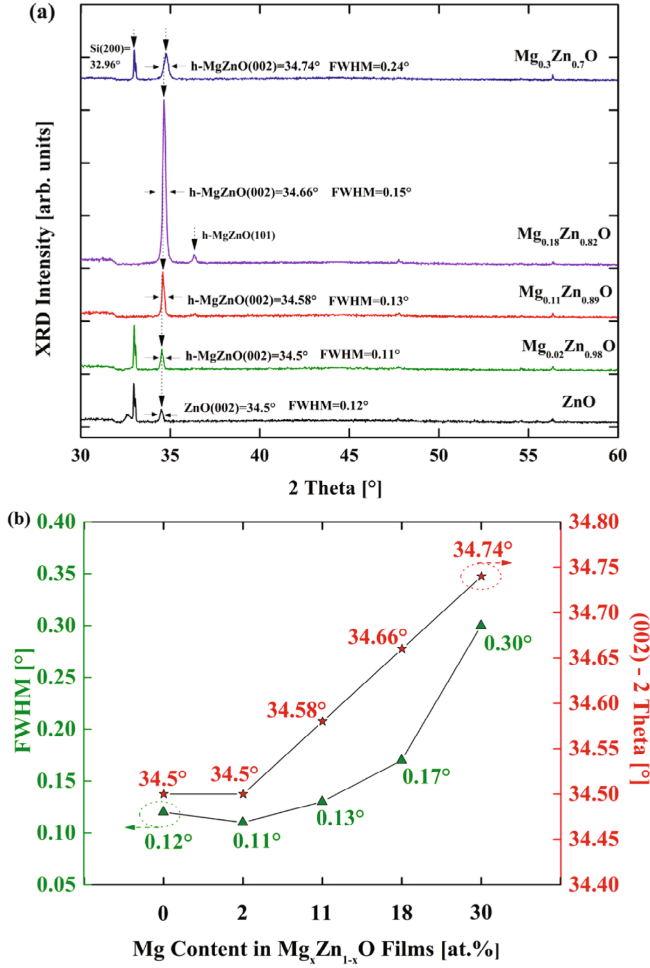

Fig. 1. (Color online) (a) XRD θ-2θ patterns for the ZnO, $Mg_{0.02}Zn_{0.98}O$, $Mg_{0.11}Zn_{0.89}O$, $Mg_{0.18}Zn_{0.82}O$, and $Mg_{0.3}Zn_{0.7}O$ films and (b) XRD results of the $Mg_xZn_{1-x}O$ films as a function of the Mg concentration.

$Mg_xZn_{1-x}O$/ZnO (x = 0.8, 0.16) heterojunction by co-sputtering with ZnO and MgO targets. The ZnO and the MgO co-sputtering are widely used. However, without a buffer layer, the maximum Mg content of $Mg_xZn_{1-x}O$ films deposited by co-sputtering with ZnO and MgO targets on Si (001) substrates was only 7 at.% [13], even though a relatively high RF power was applied to the MgO target. Because the MgO target has a very low sputtering yield, the MgO target is difficult to sputter. Therefore, good-quality wurtzite $Mg_xZn_{1-x}O$ films with high Mg content are rare.

In our case, we used RF magnetron co-sputtering with wurtzite ZnO and $Mg_{0.3}Zn_{0.7}O$ targets to deposit $Mg_xZn_{1-x}O$ films on Si substrates. Ohtomo *et al.* [8] reported that wurtzite $Mg_xZn_{1-x}O$ films could be maintained to 33 at.%, so we expect to co-sputter the $Mg_{0.3}Zn_{0.7}O$ and the ZnO targets to deposit wurtzite $Mg_xZn_{1-x}O$ films with Mg contents ranging from 0 at.% to 30 at.%. Moreover, the $Mg_{0.3}Zn_{0.7}O$ target has a higher sputtering yield than the MgO target, so increasing the incorporation ratio of Mg into ZnO is possible. Thus by co-sputtering ZnO and $Mg_{0.3}Zn_{0.7}O$ targets, the Mg content could be varied from 0 at.% to 30 at.% by varying the RF power applied to the $Mg_{0.3}Zn_{0.7}O$ target. The microstructural properties were characterized by using X-ray diffraction (XRD) and atomic force microscopy (AFM). The electrical properties of the $Mg_xZn_{1-x}O$ films as functions of the Mg content were investigated by using the transmission line model (TLM) and Hall effect measurements.

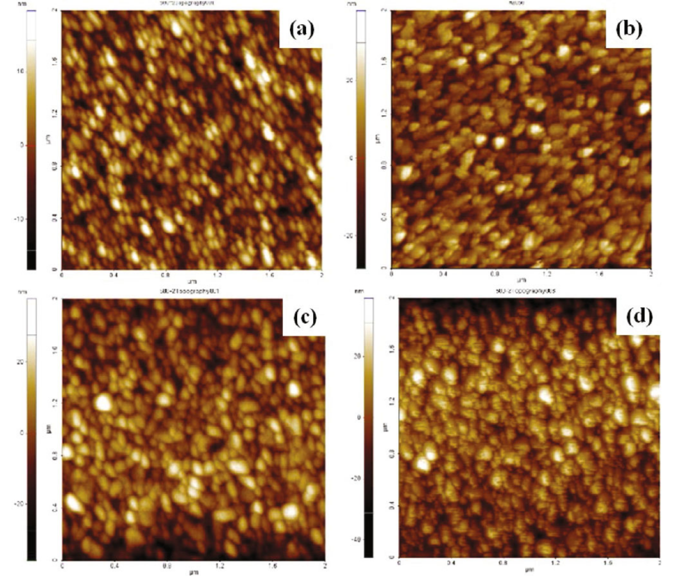

Fig. 2. (Color online) Surface morphologies for the (a) ZnO, (b) $Mg_{0.02}Zn_{0.98}O$, (c) $Mg_{0.11}Zn_{0.89}O$, and (d) $Mg_{0.18}Zn_{0.82}O$ films.

II. EXPERIMENTS

The ternary $Mg_xZn_{1-x}O$ films were deposited on n-Si (100) substrates by RF magnetron co-sputtering. Silicon substrates yield a resistivity of 0.5 – 8 Ω·cm in conjunction with an n-type carrier. The co-sputtered commercial targets, ZnO and $Mg_{0.3}Zn_{0.7}O$ (4-inch diameter, Mg/(Mg+Zn) = 30 at.%), had a purity of 99.99%. Before the Si substrates were loaded into the sputtering chamber, they had been cleaned with acetone, methanol, and de-ionized water in an ultrasonicator for 15 min. The base pressure was less than 10^{-6} Torr, and the working pressure was 5 mTorr. Argon gas was introduced at a flow rate of 20 cm^3/min, which was controlled by using a mass flow controller. The ZnO and the $Mg_xZn_{1-x}O$ films were deposited for 90 min at 300 °C. The RF power of ZnO target was 100 W, which remained unchanged, whereas the power applied to $Mg_{0.3}Zn_{0.7}O$ target was set to 0 W, 50 W, 100 W, and 150 W, and the corresponding samples were designated as ZnO, MZO50, MZO100, and MZO150, respectively. The $Mg_xZn_{1-x}O$ films were

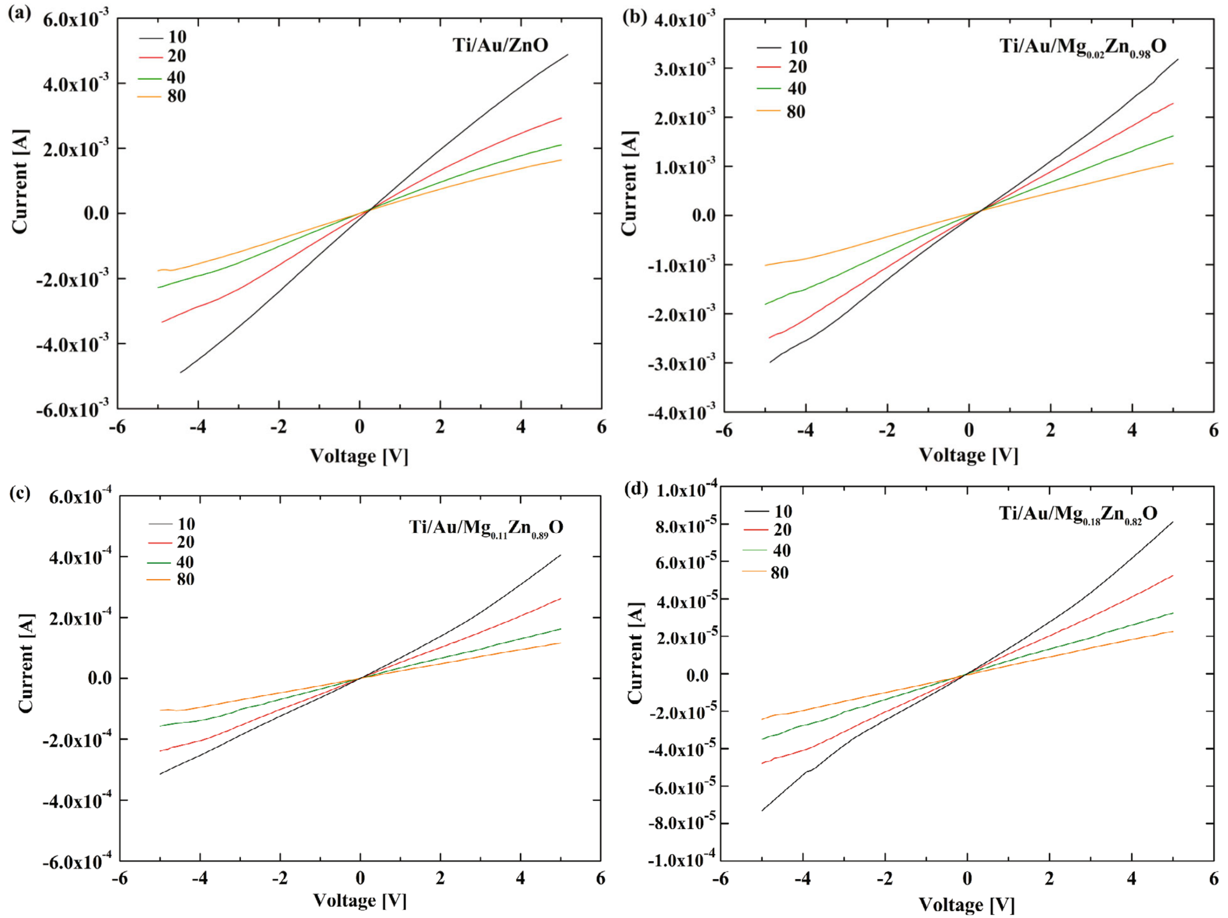

Fig. 3. (Color online) *I-V* characteristic of Ti/Au contacts on (a) ZnO, (b) $Mg_{0.02}Zn_{0.98}O$, (c) $Mg_{0.11}Zn_{0.89}O$, and (d) $Mg_{0.18}Zn_{0.82}O$ films in the −5 V ∼ 5 V voltage range and measured by using the transmission line model.

deposited to 180 nm (ZnO), 260 nm (MZO50), 310 nm (MZO100), and 330 nm (MZO150), respectively. After deposition, all the samples were annealed at 750 °C in an O_2 ambient for 60 min. Then, the TLM pattern with a series of Ti (10 nm)/Au (50 nm) contacts, which had been deposited by using the e-beam evaporation system and post-annealed at 500 °C in vacuum for 60 s by using a rapid thermal process, was formed by using a photolithography method.

The Mg concentration was confirmed by using an energy dispersive X-ray analysis (EDAX, Tescan, MIRA-3). The structural characteristics were investigated by using XRD (Rigaku, Smartlab) spectrum, and the surface morphologies were measured by using AFM (Park systems, XE-100). The current-voltage (*I-V*) characteristics were measured by using a semiconductor parameter analysis (Hewlett-Packard, HP-4145B), and the electrical properties were evaluated by using Hall effect measurements (Ecopia, HMS-5000).

III. RESULTS AND DISCUSSION

The Mg compositions in MZO50, MZO100, and MZO150 were confirmed as 2 at.%, 11 at.%, and 18 at.%, respectively. Figure 1(a) shows the XRD diffraction patterns of ZnO, $Mg_{0.02}Zn_{0.98}O$, $Mg_{0.11}Zn_{0.89}O$, and $Mg_{0.18}Zn_{0.82}O$ films. All samples predominantly show the (002) direction with a hexagonal wurtzite structure. The ZnO (002) diffraction peak is 34.5° whereas the $Mg_{0.02}Zn_{0.98}O$, $Mg_{0.11}Zn_{0.89}O$, and $Mg_{0.18}Zn_{0.82}O$ films respectively display a hexagonal MgZnO (002) peak at 34.5°, 34.58°, and 34.66°, which shifts to 34.74° for the single $Mg_{0.3}Zn_{0.7}O$ target (as shown in Fig. 1(b)). The increased Bragg diffraction angle indicates a decrease in the *c*-axis lattice constant owing to the substitution of Mg ions with smaller ionic radius at the Zn sites. The replaced ratio increases with increasing Mg content. Owing to the difference between the radii of Mg^{2+} and Zn^{2+}, the full widths at half maxima (FWHMs) of the $Mg_xZn_{1-x}O$ films increase as the Mg concentration is increased.

Figure 2 shows the AFM results for the $Mg_xZn_{1-x}O$ films. The surfaces of the $Mg_xZn_{1-x}O$ films reveal grain-shaped islands. The grain sizes for ZnO, $Mg_{0.02}Zn_{0.98}O$,

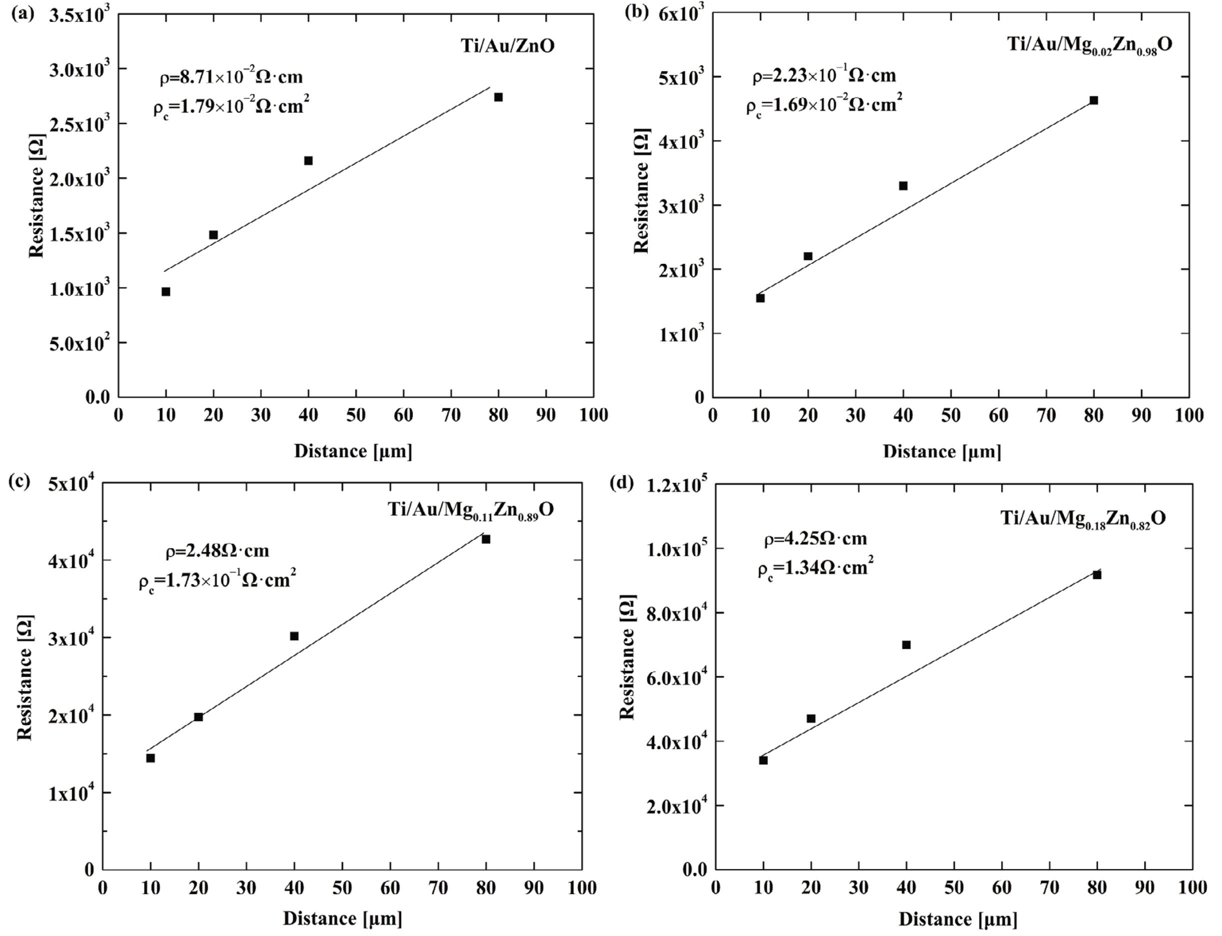

Fig. 4. Resistance-distance correlation of Ti/Au contacts on (a) ZnO, (b) $Mg_{0.02}Zn_{0.98}O$, $Mg_{0.11}Zn_{0.89}O$, and (d) $Mg_{0.18}Zn_{0.82}O$ films measured by using the transmission line model. The resistance is derived from the *I-V* curve in the -5 V $\sim$ 5 V voltage range.

$Mg_{0.11}Zn_{0.89}O$, and $Mg_{0.18}Zn_{0.82}O$ are 79.9 nm, 75.2 nm, 83.7 nm, and 89.7 nm, respectively. With increasing Mg content, the grain size increases. The value of the root-mean-square (RMS) roughness is from 4.5 nm to 7.6 nm.

Figure 4 shows the resistance as a function of the distance between two adjacent contacts. The resistance was calculated according to the *I-V* curve (-5 V $\sim$ 5 V) in Fig. 3 and the straight line in Fig. 4 was fitted by using a the linear squares method. According to the TLM method [14], the total resistance, R, between two adjacent contacts is given by:

$$R(d_i) = 2R_c + (R_S/W)d_i, \quad (1)$$

where R_c denotes the contact resistance, W the width of the contact, and R_s the sheet resistance of the semiconductor layer outside the contacts. Thus, the special contact resistivity can be obtained as:

$$\rho_c = (R_c^2 W^2)/R_S, \quad (2)$$

and the bulk film resistivity can be evaluated by using:

$$\rho = R_S \cdot h, \quad (3)$$

where h denotes the thickness of the $Mg_xZn_{1-x}O$ films.

The special contact resistivity increases from 1.79 $\times$ 10^{-2} Ω·cm^2 to 1.34 Ω·cm^2 as the Mg content is increased from 0 at.% to 18 at.% as shown in Fig. 5. According to Fig. 5, the resistivity of ZnO, $Mg_{0.02}Zn_{0.98}O$, $Mg_{0.11}Zn_{0.89}O$, and $Mg_{0.18}Zn_{0.82}O$ films are 8.71 $\times$ 10^{-2} Ω·cm, 2.23 $\times$ 10^{-1} Ω·cm, 2.48 Ω·cm, and 4.25 Ω·cm, respectively. The resistivity increases for the films with increasing Mg concentration, which is consistent with the results of the Hall effect measurements (as shown in Fig. 6). This may result from the substitution of Mg ions with a smaller ionic radius at the Zn sites. The increased number of Mg ions cause more lattice distortion, which increases the lattice scattering. Similarly, Chen *et al.* also observed an increase in the resistivity of Mn-doped ZnO with increasing Mn concentration [15].

Figure 6 shows the results of the Hall effect measurements, which were made at room temperature. The electron concentrations of ZnO, $Mg_{0.02}Zn_{0.98}O$, $Mg_{0.11}Zn_{0.89}O$, and $Mg_{0.18}Zn_{0.82}O$ were 1.17 $\times$ 10^{19} cm^{-3}, 2.84 $\times$ 10^{18} cm^{-3}, 3.14 $\times$ 10^{17} cm^{-3}, and 1.17 $\times$ 10^{17} cm^{-3} respectively, and decrease significantly with

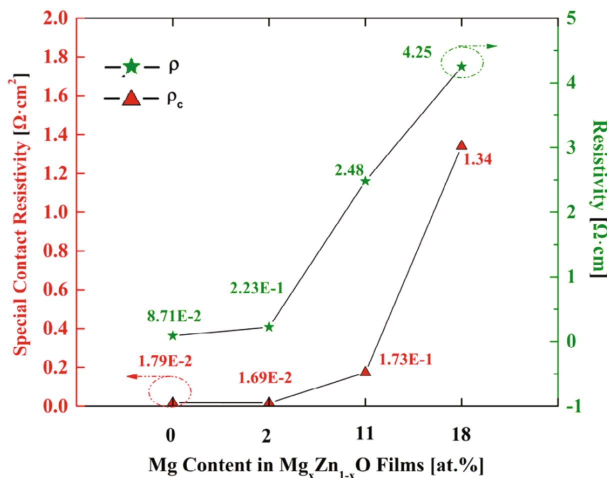

Fig. 5. (Color online) Special contact resistivity and resistivity of $Mg_xZn_{1-x}O$ films as functions of the Mg concentration, and measured by using the transmission line model.

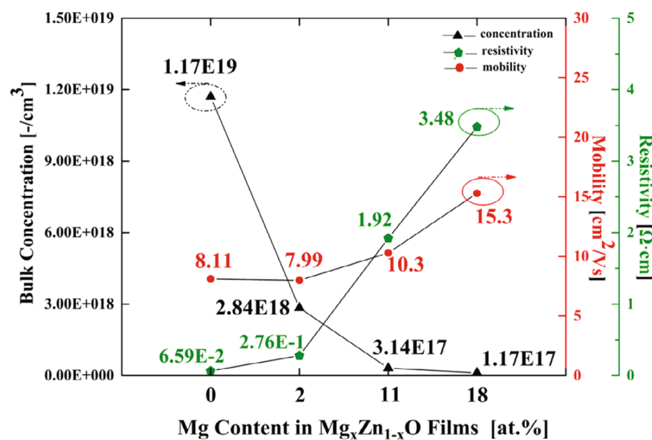

Fig. 6. (Color online) Carrier concentration, mobility and resistivity of $Mg_xZn_{1-x}O$ films as functions of the Mg concentration, and obtained by using Hall effect measurements.

increasing Mg concentration. This indicates that the incorporation of Mg into ZnO reduces the formation of oxygen vacancies due to the strong interaction between the Mg^{2+} ions and the O^{2-} ions. A similar relation between the carrier concentration and the number of oxygen vacancies in ZnO:$Ga_{0.004}$ thin film was found by Lorenz *et al.* [16]. The decrease in the number of oxygen vacancies, which act as donors under the ohmic contact, explains why the special contact resistivity increases as the Mg content is increased. As the carrier concentration decreases from 1.17×10^{19} cm^{-3} to 1.17×10^{17} cm^{-3}, the Hall mobility increases from 8.11 cm^2/Vs to 15.3 cm^2/Vs. Even though the carrier concentration is reduced to 0.01 times that of ZnO as the Mg concentration is increased to 18 at.%, the mobility is only increased to 2 times that of ZnO, which indicates that the incorporation of Mg into ZnO causes lattice distortion which explains why the resistivity of the $Mg_xZn_{1-x}O$ films increases with increasing Mg content. Klüpfel *et al.* [17] successfully fabricated a metal semiconductor field-effect transistor (MESFET) based on a ZnO:Mg thin film grown by using pulsed laser deposition on α-plane sapphire, in which the Hall mobility of the thin film was 10 cm^2/Vs. In our case, the Hall mobility of $Mg_{0.11}Zn_{0.89}O$ and $Mg_{0.18}Zn_{0.82}O$ are higher than 10 cm^2/Vs. Transistors made from materials with high mobility generally have better properties than those made from lower mobility material. Thus $Mg_xZn_{1-x}O$ ($0 \leq x \leq 0.18$) films display good electrical properties and are promising for future applications in optoelectronic devices.

IV. CONCLUSION

We successfully deposited $Mg_xZn_{1-x}O$ films with a maximum Mg content of 18 at.% on Si substrates by using RF magnetron co-sputtering with ZnO and $Mg_{0.3}Zn_{0.7}O$ targets. The $Mg_xZn_{1-x}O$ films predominantly showed the (002) direction with a hexagonal wurtzite structure and no phase separation. The electrical properties of the $Mg_xZn_{1-x}O$ films were tuned by using the Mg content. With increasing Mg content, the resistivity increased, and the carrier concentration decreased from 1.17×10^{19} cm^{-3} to 1.17×10^{17} cm^{-3}, indicating a the reduction in the number of oxygen vacancies. Meanwhile, the Hall mobility increased as the carrier concentration decreased. The Hall mobility of $Mg_{0.11}Zn_{0.89}O$ and $Mg_{0.18}Zn_{0.82}O$ were 10.3 and 15.3 cm^2/Vs, which were higher than the reported value [17]. Thus $Mg_xZn_{1-x}O$ ($0 \leq x \leq 0.18$) films own good structural and electrical properties, which made them promising for future applications in optoelectronic devices.

ACKNOWLEDGMENTS

This research was supported by the Basic Science Research Program through the National Research Foundation of Korea (NRF) funded by the Ministry of Education, Science and Technology (2012R1A1A4A01011424).

REFERENCES

[1] S. Lee, Y. Lee, D. Y. Kim, E. B. Song and S. M. Kim, Appl. Phys. Lett. **102**, 242114 (2013).

[2] F. Fang, J. Futter, A. Markwitz and J. Kennedy, Nanotechnology **20**, 245502 (2009).

[3] P. I. Reyes, C.-J. Ku, Z. Duan, Y. Lu, A. Solanki and K.-B. Lee, Appl. Phys. Lett. **198**, 173702 (2011).

[4] P.-N. Ni, C.-X. Shan, B.-H. Li and D.-Z. Shen, Appl. Phys. Lett. **104**, 032107 (2014).

[5] D. K. Hwang, M. C. Jeong and J. M. Myoung, Appl. Surf. Sci. **225**, 217 (2004).

[6] X. Chen and J. Kang, Semicond. Sci. Tech. **23**, 025008 (2008).
[7] E. R. Segnit and A. E. Holland, J. Am. Ceram. Soc. **48**, 409 (1965).
[8] A. Ohtomo, M. Kawasaki, T. Koida, K. Masubuchi, H. Koinuma, Y. Sakurai, Y. Yoshida, T. Yasuda and Y. Segawa, Appl. Phys. Lett. **72**, 2466 (1988).
[9] C. W. Lin, T. Y. Cheng, L. Chang and J. Y. Juang, Phys. Status Solidi C **1**, 851 (2004).
[10] G. Srinivasan and J. Kumar, Cryst. Res. Technol. **41**, 893 (2006).
[11] Y. Y. Kim, B. H. Kong, M. K. Choi and H. K. Cho, Mater. Sci. Eng. B **165**, 80 (2009).
[12] J. P. Kar, M. C. Jeong, W. K. Lee and J.M. Myoung, Mater. Sci. Eng. B **147**, 74 (2008).
[13] S. W. Kang, Y. Y. Kim, C. H. Ahn, S. K. Mohanta and H. K. Cho, J. Mater. Sci.: Mater. Electron. **19**, 755 (2008).
[14] C. Y. Hu *et al.*, Mater. Sci. Eng. B **128**, 37 (2006).
[15] W. Chen, J. Wang and M.-R. Wang, Vacuum **81**, 894 (2007).
[16] M. Lorenz *et al.*, Solid-State Electron. **47**, 2205 (2003).
[17] F. J. Klüpfel, H. von Wenckstern and M. Grundmann, Appl. Phys. Lett. **106**, 033502 (2015).